HHS Public Access

Author manuscript

Structure. Author manuscript; available in PMC 2019 November 06.

Published in final edited form as:

Structure. 2018 November 06; 26(11): 1451–1461.e4. doi:10.1016/j.str.2018.07.015.

The N-terminal GTPase domain of p190RhoGAP proteins is a pseudoGTPase

Amy L. Stiegler[1] and **Titus J. Boggon**[*,1,2,3,4]

[1]Department of Pharmacology, Yale University School of Medicine, 333 Cedar Street, New Haven, CT, 06520, USA.

[2]Department of Molecular Biophysics and Biochemistry, Yale University School of Medicine, 333 Cedar Street, New Haven, CT, 06520, USA.

[3]Yale Cancer Center, Yale University School of Medicine, 333 Cedar Street, New Haven, CT, 06520, USA.

[4]Lead contact

Summary

The pseudoGTPases are a rapidly growing and important group of pseudoenzymes. p190RhoGAP proteins are critical regulators of Rho signaling and contain two previously identified pseudoGTPase domains. Here we report that p190RhoGAP proteins contain a third pseudoGTPase domain, termed N-GTPase. We find that GTP constitutively purifies with the N-GTPase domain, and a 2.8 Å crystal structure of p190RhoGAP-A co-purified with GTP reveals an unusual GTP-Mg^{2+} binding pocket. Six inserts in N-GTPase indicate perturbed catalytic activity and inability to bind to canonical GAP, GEF and effector proteins. Biochemical analysis shows that N-GTPase does not detectably hydrolyze GTP, and exchanges nucleotide only under harsh Mg^{2+} chelation. Furthermore, mutational analysis shows that GTP and Mg^{2+} binding stabilizes the domain. Therefore, our results support that N-GTPase is a nucleotide binding, non-hydrolyzing, pseudoGTPase domain that may act as a protein-protein interaction domain. Thus, unique among known proteins, p190RhoGAPs contain three pseudoGTPase domains.

Graphical Abstract

[*]Correspondence: titus.boggon@yale.edu.

Author contributions

Methodology, Investigation, Validation, Formal Analysis, Writing – Original Draft: A.L.S.; Conceptualization, Visualization, Writing – Review & Editing: A.L.S. and T.J.B.; Supervision, Project Administration, Funding Acquisition: T.J.B.

Declaration of Interests

The authors declare no competing financial interests.

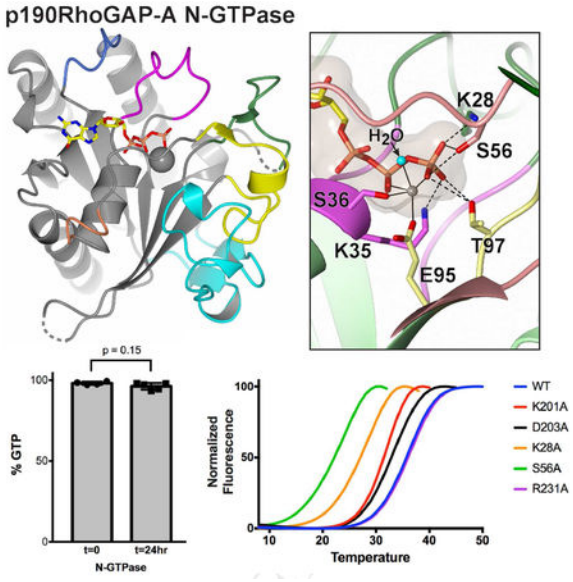

Introduction

‘Pseudoenzymes’ comprise an estimated 10-15% of known members of most enzyme classes (Murphy et al., 2017a; Pils and Schultz, 2004). These proteins adopt the overall fold of their respective enzyme families but are sequentially divergent in conserved enzymatic residues. This often results in partial or complete deficiencies in catalytic activity (Eyers and Murphy, 2016). Nonetheless, pseudoenzymes can function in signal transduction pathways as adaptors or regulators of signaling, and the study of these proteins has lead to a better understanding of the roles of enzymatic folds beyond catalysis (Murphy et al., 2017b). The best studied pseudoenzymes are the pseudokinases (Boudeau et al., 2006), which were identified by genome-wide sequence analyses that revealed kinases lacking one or more of the conserved amino acid motifs responsible for catalytic activity (Manning et al., 2002). Similarly, a number of pseudoenzymes within the Ras superfamily of small GTPases have been discovered (Basilico et al., 2014; Foster et al., 1996; Schroeder et al., 2014; Soundararajan et al., 2007; Splingard et al., 2007; Stiegler and Boggon, 2017), and have been termed the pseudoGTPases.

Small GTPases are key regulators of cellular signaling pathways, and are classified into 5 subgroups: Ras, Rho, Rab, Ran and Arf (Wennerberg et al., 2005). These proteins undergo ‘GTP cycling’; they bind GTP, enzymatically hydrolyze the γY-phosphate of GTP to form GDP and inorganic phosphate, then release the bound GDP and phosphate to allow binding of a new GTP molecule (Vetter and Wittinghofer, 2001). Thus, GTPases act as molecular switches with ON (GTP-bound) and OFF (GDP-bound) states. GTP cycling is intrinsically slow, so facilitator proteins help accelerate specific steps of the process; hydrolysis by GTPase activating proteins (GAPs), and GDP dissociation by guanine nucleotide exchange factors (GEFs). This cycling process occurs in each of the five GTPase subgroups, and specific amino acid residues that are important for nucleotide binding and catalysis are conserved amongst the superfamily. These conserved residues are termed G motifs (G1 to

G5) (Bourne et al., 1991; Dever et al., 1987). By definition, pseudoGTPases lack, or are mutated, in one or more of the consensus G motifs (Murphy et al., 2017b).

RhoA is the founding member of the Rho subfamily of small GTPases, and plays important roles in actin reorganization, cell migration, shape, adhesion, cytokinesis, and many other cellular functions (Jaffe and Hall, 2005). Proper regulation of RhoA signaling is therefore critical for many cellular processes. Chief among RhoA regulators are the p190RhoGAP proteins, p190RhoGAP-A (ARHGAP35) and p190RhoGAP-B (ARHGAP5) (Burbelo et al., 1995; LeClerc et al., 1991; Settleman et al., 1992). These GTPase activating proteins may account for up to 60% of RhoGAP activity in the cell (Vincent and Settleman, 1999) and are critical, for example, for proper regulation of cytoskeletal structure and contractility (Arthur and Burridge, 2001; Chang et al., 1995; Ridley et al., 1993), but, surprisingly, their molecular architecture is not well studied. Within these ~170 kDa multidomain proteins we recently discovered two pseudoGTPase domains in a region previously thought to be flexible (Stiegler and Boggon, 2017) (Fig. 1a). We also found that although RhoGAP activity is primarily driven by the C-terminal GAP domain (Burbelo et al., 1995; LeClerc et al., 1991; Settleman et al., 1992) the newly discovered pseudoGTPase domains also impact RhoGAP activity (Stiegler and Boggon, 2017). These insights into p190RhoGAP proteins led us to consider whether there are further surprises hidden within their molecular architecture. We noted that upon the discovery of p190RhoGAP proteins, an N-terminal GTPase fold domain had been identified (Settleman et al., 1992). However, prior investigations of this domain yielded varying results with respect to potential nucleotide binding and/or hydrolysis activities (Foster et al., 1994; Roof et al., 2000; Tatsis et al., 1998). Therefore, we surmised that a molecular level study of this domain might provide further insights into the p190RhoGAP proteins.

Here we investigate the structural and biochemical properties of the N-GTPase domain of p190RhoGAP-A. We determine the crystal structure and find that N-GTPase adopts an extended GTPase-like fold with six unique inserts that seem to preclude its ability to bind typical GAP, GEF or effector molecules. We find that N-GTPase is bound constitutively to GTP/Mg^{2+} and lacks intrinsic catalytic activity. We also use mutational analysis to show that GTP and Mg^{2+} binding stabilizes the domain. Therefore, our study supports both that p190RhoGAP N-GTPase is a nucleotide binding, non-hydrolyzing, pseudoGTPase domain that cannot bind canonical GAP, GEF or effector proteins, that may act as a protein-protein interaction module. Unique among known proteins, the p190RhoGAPs contain three pseudoGTPase domains.

Results

Expression and crystallization of p190RhoGAP N-GTPase domain

We expressed the isolated N-GTPase domain of p190RhoGAP-A recombinantly in *E. coli* and purified to homogeneity to conduct biochemical and structural studies (Fig. 1a and Supplemental Fig. 1a,b). We crystallized the purified protein without addition of nucleotide at any purification or crystallization step, and determined its 2.8 Å crystal structure. The structure contains two copies of the N-GTPase domain per asymmetric unit (Table 1). One copy (termed copy A) exhibits good electron density and allowed model building for 231 of

271 total residues. The second copy (B) is less well ordered, with poorer electron density and higher average *B*-factors, allowing only 187 residues to be built (Table 1 and Supplemental Fig. 1c), nonetheless, the two copies superpose well with root-mean-squared deviation (R.M.S.D.) of 0.6 Å between 187 equivalent Cα positions. In this study, we use the better resolved copy A for detailed structural analysis.

p190RhoGAP N-GTPase domain adopts an extended GTPase domain fold

The crystal structure of p190RhoGAP N-GTPase domain reveals a characteristic GTPase-like core (Bourne et al., 1991), with a central beta sheet comprised of six strands (β1-β6; 5 parallel and one antiparallel) surrounded by five helices (α1-α5) and a GTP/Mg^{2+} pair at the predicted binding site (Fig. 1b). Additionally, N-GTPase contains multiple unique insert sequences which contribute to an overall extended GTPase domain (Fig. 1b,c **and** Supplemental Fig. 2). A search using the Dali server (Holm and Rosenstrom, 2010) reveals the closest related structures are of small GTPases in the Ras subfamily (e.g., R.M.S.D. 2.1 Å over 152 residues (PDB ID 1Q21, H-Ras (Tong et al., 1991)), Fig. 1c), which share approximately 25% sequence identity with N-GTPase (Fig. 2). Notably, most of the residues conserved between N-GTPase and H-Ras are located in the hydrophobic core.

The length of the N-GTPase inserts range between 3 to 31 amino acid residues. These inserts (termed insert-1 to -6) are unique when structurally superposed with other small GTPases (Fig. 1c, Fig. 2, **and** Supplemental Fig. 2, and in 3-dimensional space are contiguous with one another (with the exception of insert-2). The inserts bury a large area of the GTPase core domain (approximately 1700 $Å^2$), which is over 20% of the total core GTPase surface. These inserts therefore significantly alter the surface shape of the GTPase domain (Fig. 3a,b). Importantly, rather than long flexible loops that simply connect core GTPase elements, these insert regions interact intimately with both the GTPase core and with each other, and form multiple secondary structure features (Fig. 2 and Fig. 3). By Dali search, no structural homologs of this region could be identified (Holm and Rosenstrom, 2010). The sequences of the inserts are evolutionarily well conserved in p190RhoGAP-A, and are also present in p190RhoGAP-B and the p190RhoGAP proteins of more ancestral eukaryotic species (Fig. 2). Thus, the crystal structure shows that the unique N-GTPase inserts form an intrinsic part of the N-GTPase domain fold, and reveals that structurally, p190 N-GTPase is an extended GTPase domain.

The inserts in N-GTPase consist of insert-1: an extended G1 P-loop (between β1-α1); insert-2: a short extended loop at the end of α1; insert-3: preceding β2; insert-4: between β3-α2; insert-5: between α2-β4, the longest insert at 33 residues; and insert-6: between β4-α3 (Figs. 2 and 3). In the structure, the inserts are arranged in the following order on the surface: insert-6/-1/-4/-3/-5/-2 (Fig. 3a). Specifically, insert-6 is tethered to the GTPase core and to insert-1 via the sidechain of Arg-172 (Fig. 3c). Notably, insert-1 makes direct contact with GTP (Fig. 3c), which we discuss further below. Insert-1 and insert-4 associate via several van der Waals interactions (not shown). A short 2-stranded parallel beta sheet connects insert-3 (β1 i) and insert-4 (β2i), while His-108 in insert-4 further links to insert-3 (Leu-58) and to the GTPase core (His-72) through H-bonds (Fig. 3d). Insert-3 and insert-4 also contribute numerous hydrophobic sidechains to the core of the fold including Leu-58,

Phe-63 and Phe-99 (Fig. 3d) as well as Val-67 and Val-68 (Fig. 3e). The longest insert, insert-5, extends as a beta-hairpin approximately 30 A along the GTPase domain surface (Fig. 3e). It is anchored by two short beta strands (β3i-β4i) and a network of hydrogen bonds involving residues 127-131 with Arg-66, Asn-69, and Asp-71 (Fig. 3e). At the other end of insert-5, Tyr-133 plugs into the hydrophobic core; its sidechain makes a hydrogen bond with His-54, while its backbone bonds with the sidechain of Arg-44 (Fig. 3f) to stabilize the local structure. Together, this network of interactions reflect that the insert sequences are an intrinsic part of the overall fold of the N-GTPase domain.

N-GTPase binds GTP constitutively and lacks hydrolysis activity

Our purification protocol for N-GTPase did not include addition of any nucleotide, however, in the crystal structure we observe clear electron density corresponding to both GTP and Mg^{2+} at the expected binding site (Fig. 4a,b,c). Therefore we assessed the phospho-species of nucleotide bound to the pool of purified N-GTPase protein by strong anion exchange chromatography (Ogita et al., 2015; Zavialov et al., 2001), and find that N-GTPase is bound predominantly to GTP (Fig. 4d). This is in clear contrast to wild-type Rac1 which, like other active GTPases, is bound predominantly to GDP due to its inherent hydrolysis activity (Fig. 4d) (Smith and Rittinger, 2002). Instead, N-GTPase is similar to the pseudoGTPase Rnd3, which binds only GTP (Fig. 4d) since it lacks intrinsic hydrolysis activity (Foster et al., 1996).

Our finding that N-GTPase purifies in its GTP-bound form strongly suggests that, like Rnd3, it lacks intrinsic hydrolysis activity. To test this experimentally, we incubated purified N-GTPase in the presence of Mg^{2+} and measured the conversion of GTP to GDP by separating them on strong anion exchange chromatography. These results show that N-GTPase does not hydrolyze GTP to GDP, whereas Rac1 (preloaded with GTP) exhibits complete hydrolysis of GTP to GDP in identical conditions (Fig. 4e). Taken together, our structural and biochemical studies support the conclusion that N-GTPase binds GTP yet is catalytically inactive, which classifies it as a pseudoGTPase.

N-GTPase is resistant to GTP exchange *in vitro*

Since the p190RhoGAP N-GTPase domain is bound predominantly to GTP and exhibits no catalytic competency *in vitro*, we next studied its GTP exchange properties using a fluorescence-based MANT-GTP ((2'/3')-*O*-(*N*-Methyl-anthraniloyl)-guanosine 5'-triphosphate) binding assay. As shown by others (Hall and Self, 1986) and confirmed here, typical small GTPases like H-Ras (G12V used here) readily exchange bound nucleotide with MANT-GTP in solution (Fig. 4f); however, exchange is slowed at physiological Mg^{2+} concentrations (1 mM (Romani, 2011)), which can be overcome by further addition of EDTA (2mM) (Fig. 4f). Overall, this exchange behavior is due to excess Mg^{2+} stabilizing the closed nucleotide-bound conformation; *in vitro*, EDTA chelates the tightly-bound Mg^{2+} and allows nucleotide exchange, while *in vivo*, a GEF is needed to stimulate exchange (Lin et al., 1997). In this way, Mg^{2+} acts as a gatekeeper to activation (Hall and Self, 1986; Zhang et al., 2000).

Remarkably, for p190 N-GTPase we observe that GTP to MANT-GTP exchange occurs very slowly in both the basal condition and at 1 mM Mg^{2+}/2 mM EDTA where typical GTPases readily exchange nucleotide (Fig. 4g). This behavior suggests that the GTP-bound conformation of N-GTPase is more favored compared to typical GTPases. This is further supported by our finding that EDTA concentrations of 20 mM in combination with 10 mM Mg^{2+} (tenfold higher than are needed for typical GTPases) are required to overcome the gatekeeper effect of bound Mg^{2+} and promote GTP exchange (Fig. 4g). These results support the idea that the N-GTPase complex with GTP/Mg^{2+} is very stable.

Structural basis for GTP binding and lack of catalytic activity

Examination of the GTP/Mg^{2+} binding site in our crystal structure of N-GTPase reveals numerous differences when compared to typical GTPases such as H-Ras. Typical small GTPases contain five conserved ‘G motifs’ whose consensus sequences confer GTP/Mg^{2+} binding and catalytic activity (Wennerberg et al., 2005). In N-GTPase, three of these G motifs are disrupted by the insert sequences: G1 by insert-1, G2 (Switch I) by insert-3 and G3 (Switch II) by insert-4 (Fig. 2 and Fig. 5a-b). In contrast, G4 and G5 are conserved in N-GTPase; together, they form the binding pocket for the guanine base and are responsible for specificity of guanine over adenosine nucleotides (Bourne et al., 1991) (Fig. 2 and Fig. 5a-b).

At the structural level, many of the differences we observe between N-GTPase and typical small GTPases can provide a rationale for both constitutive GTP binding and lack of hydrolysis activity. Most notably, the catalytic glutamine (Q61 in H-Ras) is missing in N-GTPase. In H-Ras, mutation of H-Ras Q61 results in deficient GTP hydrolysis (Der et al., 1986), and similarly, lack of a glutamine at the equivalent position in Rnd3 (Ser-66) is partly responsible for Rnd3’s lack of activity (Foster et al., 1996). We find that in the structure-based sequence alignment of N-GTPase (Fig. 2) this glutamine residue is replaced by Ala-112 (which is disordered in our structure); however, in 3-dimensional space, the Q61 position is occupied by the Ser-Gly-Thr from insert-1 (residues 22-24) and Glu-98 from Switch II (Fig. 5c). The replacement of a glutamine residue in 3-dimensional space by these two features therefore implies direct impact on catalytic activity.

We find two further major structural differences: in the coordination of the GTP gamma phosphate and in the coordination of Mg^{2+}. For the gamma phosphate, residues Lys-28, Ser-56 and Thr-97 each make direct interactions that are not observed in canonical small GTPases (Fig 5d and 5e). For the Mg^{2+} binding site, two of the six potential coordination sites are highly divergent from canonical small GTPases. First, Glu-95 in N-GTPase directly coordinates the Mg^{2+} cation and replaces the highly conserved catalytic Asp-57 from H-Ras which instead stabilizes a water molecule that coordinates Mg^{2+} (Fig 5e). Second, in H-Ras, the sidechain of invariant Thr-35 in Switch I directly coordinates the Mg^{2+}; in N-GTPase, no protein sidechain is in close enough proximity to directly coordinate the cation; instead, we predict that a water molecule, poorly ordered in our 2.8 Å crystal structure, provides Mg^{2+} coordination at this site.

N-GTPase stability requires GTP binding

Notably, the GTP- and Mg^{2+}-binding residues of N-GTPase are largely conserved (Fig 5d and 2). In order to probe their role in N-GTPase, we performed mutagenesis and expressed the mutant proteins recombinantly in *E. coli*, in hopes to biochemically probe GTP binding. We find that for several mutants, no soluble protein is obtained despite sufficient expression at the whole-cell level (Fig. 5f and Supplemental Fig. 3). Thus, these mutations render the recombinant N-GTPase protein insoluble, suggesting that GTP binding is necessary for the structural integrity of the domain. However, some mutations such as K201A, D203A, R231A, K28A or S56A, allowed for purification of recombinant protein (Fig. 5g). We therefore assessed the stability of these mutant proteins by differential scanning fluorimetry and compared their melting temperatures to wild-type N-GTPase (Fig. 5h,i). We find that mutations K201A and D203A, both in the conserved G4 motif that binds the guanine base of GTP (Fig. 5a, 5d), cause a modest but significant decrease in the melting temperature of N-GTPase compared to wild-type (Fig. 5h,i) using a thermal denaturation assay ((Murphy et al., 2014) and we postulate that this indicates a weakening of the interaction with nucleotide. More dramatically destabilized are the N-GTPase mutants K28A in insert-1 (that disrupts the P-loop) and S56A in Switch I (Fig. 5d), which show much lower melting temperatures compared to wild-type (Fig. 5h,i). In contrast, R231A from the G5 motif, whose side chain does not directly interact with GTP, exhibits the same melting temperature as wild-type (Fig. 5 h,i). These results support that GTP binding to N-GTPase stabilizes the fold of the domain.

GAP, GEF, and effector binding sites are sterically blocked in N-GTPase

Our above analysis of p190RhoGAP N-GTPase finds that this domain intrinsically interacts with GTP, and has no catalytic activity, and exchanges extremely slowly. The structure also shows six unusual inserts that extend the small GTPase domain in regions proximal to the nucleotide binding site. We therefore wondered whether the structure of the N-GTPase domain would suggest that GAP, GEF or effector proteins could bind. To test this we superposed small GTPase structures in complex with their cognate GAPs, GEFs or effector proteins onto N-GTPase. In each case we observe extensive predicted steric clashes that are expected to block binding of these molecules to N-GTPase (Fig. 6).

Typical GAPs for small GTPases bind and insert an “Arginine finger” into the catalytic cleft that is required for GAP-mediated catalysis (Ahmadian et al., 1997; Scheffzek et al., 1997). In N-GTPase, Lys-28 from insert-1 blocks the putative Arg-finger site, and the remainder of the GAP binding site is blocked by the insert regions (Fig 6b). Therefore, it is unlikely that a standard GAP would promote hydrolysis activity in N-GTPase. Similarly, binding of GEF molecules to facilitate nucleotide exchange is predicted to be sterically blocked by the insert regions of N-GTPase (Fig 6c), and many effector molecules would be blocked by the N-GTPase inserts (Fig 6d). Taken together, results from these structural analyses support that N-GTPase is unlikely to bind GAP, GEF, or effector molecules in standard ways. However, the existence of non-canonical interaction partners for p190RhoGAP cannot be ruled out.

Discussion

The p190RhoGAP proteins are two of the most important regulators of Rho GTPase signaling. However, surprisingly, although these proteins were identified almost 30 years ago much remains to be learnt about their molecular level details. For example, recently we discovered that within the putative unfolded ‘middle domain’ of the p190RhoGAPs there are two nonnucleotide binding pseudoGTPase domains (Stiegler and Boggon, 2017) (pG1 and pG2, Fig. 1a). We therefore decided to probe the molecular level details of the N-terminal GTPase domain. In the present study, we show that this domain is a nucleotide binding, non-hydrolyzing, pseudoGTPase domain. Furthermore, our study strongly suggests that this domain cannot bind canonical GAP, GEF or effector proteins in the usual manner. These results therefore firmly place the p190RhoGAP N-GTPase domain in the pseudoGTPase group.

Pseudoenzymes corresponding to active enzymes that catalyze nucleotide reactions, such as pseudokinases and pseudoGTPases, can be classified into three groups: those that cannot bind nucleotide, those that can bind but have no or very weak catalytic activity, and those with retained catalytic activity ((Murphy et al., 2014). These are classified as groups i, ii and iii, respectively (Table 2). Our study shows that p190RhoGAP N-GTPase is a pseudoGTPase that retains nucleotide binding activity (Table 2). Furthermore, based on our crystal structure we can now properly identify the G motifs based on structure alignment (Fig. 2), and we observe numerous changes to the G motifs. This study provides a comprehensive biophysical and biochemical analysis of the N-GTPase domain of p190RhoGAP proteins and clearly places the domain as an Rnd-like, group ii, pseudoGTPase (Table 2).

Our study adds another member to the growing list of pseudoGTPases identified by sequence and/or structural analysis. Interestingly, the list contains both single domain small pseudoGTPases (CENP-M, Rnd3 and Gem) (Basilico et al., 2014; Foster et al., 1996; Splingard et al., 2007), and now also includes pseudoGTPase domains in the multidomain p190RhoGAP proteins. This resembles the domain architectures of single domain (H-Ras, RhoA) or multidomain (GGAPs) (Xia et al., 2003) GTPases, and implies a variety of different roles in signal transduction pathways. As the search for these proteins continues, it is clear that pseudoGTPases can have very low sequence identity with typical GTPases, so sequence analysis alone is hard to use to identify new members. Furthermore, even better conserved pseudoGTPase domains such as N-GTPase can have structural features that are hard to identify in the absence of a structure. More robust secondary structure matching and structure prediction are clearly necessary to further reveal otherwise cryptic pseudoGTPase domains. As there are over 150 small GTPase superfamily proteins, we maintain that the list of pseudoGTPases will continue to grow.

Finally, the current results establish a curious and exciting result, that p190RhoGAP proteins contain three validated pseudoGTPase domains. This is extremely unusual domain composition. In the pseudokinase class, the JAKs are famous for containing both a catalytically active kinase domain and a pseudokinase domain; however, to our knowledge, no protein has been discovered that contains such a high number of pseudoenzyme domains. The reason for this architecture is unclear. We observe high conservation for all three

pseudoGTPase domains through evolution, as far back as flies and sponges (Stiegler and Boggon, 2017). One intriguing possibility is that the N-GTPase could bind in *cis* to the GAP domain at the C-terminus of p190RhoGAP to regulate its activity; however, our structural analysis predicts that this is very unlikely due to steric clashes (Fig. 6). Therefore, although there seem to be important evolutionarily conserved functional reasons for maintenance of these domains the functional roles are not yet identified. We postulate that N-GTPase acts as a protein-protein interaction scaffold or allosteric modulator. It is intriguing to further hypothesize that the unique surface on N-GTPase formed by the insert sequences provides the binding site for a potential protein partner. The presence, therefore, of three pseudoGTPase domains within the p190RhoGAP proteins provides an exciting precedent for the continued study of this exciting class of protein.

STAR METHODS

CONTACT FOR REAGENT AND RESOURCE SHARING

Further information and requests for resources and reagents should be directed to and will be fulfilled by the Lead Contact, Titus Boggon (titus.boggon@yale.edu).

EXPERIMENTAL MODEL AND SUBJECT DETAILS

All recombinant proteins were expressed in Rosetta(DE3) cells (Millipore Sigma) grown in Miller's Luria Broth base (Life Technologies) at 37°C shaking at 200 rpm in a Forma Orbital Shaker (ThermoFisher), with protein expression induced at OD_{600} = 0.6 with 0.2 mM isopropyl β-d-thiogalactopyranoside (IPTG) overnight at 16 °C with shaking.

METHOD DETAILS

Expression Constructs—The complementary DNA (cDNA) encoding full-length *Rattus norvegicus* (rat) p190RhoGAP-A (ARHGAP35) protein (NCBI Reference Sequence: NP_001258061.1, UniProt: A0A0G2KB46) was used as a PCR-template to amplify the segment encoding residues 1-266 which was inserted into pGEX-6p1 vector (GE Healthcare) for expression as a GST-fusion protein in *Escherichia coli*. A shorter N-GTPase construct of residues 13-249 was inserted into a modified pET vector for expression as a His-tagged protein. Human Rac1 (UniProt ID: P63000) cDNA encoding residues 2–177 was inserted into the pET28a plasmid for expression in *E. coli* as a His-tagged protein (Davis et al., 2013). The cDNA encoding human Rnd3 GTPase domain (UniProt ID: P61587, residues 19-200) was inserted into pGEX-6p1 (GE Healthcare). Human H-Ras (UniProt ID: P01112) residues 1-167 carrying the G12V mutation was inserted into MCS1 of pCDFDuet-1 (Millipore Sigma) for expression as an N-terminally His_6-tagged protein in *E. coli*. Site-directed mutagenesis (QuikChange Lightning, Agilent Technologies) was performed to generate point mutants. Full coding sequences were verified by DNA sequencing. Oligonucleotide sequences are listed in Table S1.

Recombinant protein expression and purification—Rosetta(DE3) cells were harvested by centrifugation for 30 min at 2,000×*g*, lysed by addition of lysozyme followed by freeze/thaw cycles and sonication. Lysates were clarified by centrifugation at 5000×*g* for 1 hr at 4°C and passed through a 0.44 μM syringe filter (Millipore) prior to affinity

purification. Cells expressing GST-p190-N-GTPase or GST-Rnd3 GTPase were lysed in glutathione-affinity lysis buffer (20 mM Tris pH 7.4, 150 mM NaCl, 5 mM dithiothreitol (DTT). Lysates were applied to Glutathione-Sepharose 4B beads (GE Healthcare) to capture GST-fusion proteins. The GST tag was removed by enzymatic cleavage with Prescission protease on-bead, and the proteins of interest further purified by size exclusion chromatography (Superdex 75, GE Healthcare) in 20 mM Tris pH 7.4 and 150 mM NaCl. Cells expressing His_6-p190-N-GTPase (wild type and mutants), His_6-Rac1, and His_6-HRas(G12V) were lysed in nickel binding buffer (50 mM HEPES pH 7.5, 500 mM NaCl, 5 mM imidazole). Lysates were applied to nickel beads (Ni-NTA Agarose, Qiagen), and bound protein eluted by increasing concentrations of imidazole in nickel-binding buffer. Elution fractions containing protein of interest were applied to size exclusion chromatography (Superdex 75 prep grade, GE Healthcare) in 20 mM Tris pH 7.4 and 150 mM NaCl. All proteins were concentrated in a centrifugal filter (Amicon Ultra, Millipore Sigma). Protein concentrations were determined by Nanodrop (ThermoFisher) at absorbance at 280nm taking into account the extinction coefficient of the primary protein sequence plus bound guanine nucleotide (7765 $cm^{-1}M^{-1}$ at 280nm) assuming a 1:1 stoichiometry.

Expression and solubility test—To test expression and solubility of mutant p190RhoGAP-A N-GTPase proteins, expression in Rosetta(DE3) cells was induced with 0.2 mM IPTG with cells at OD_{600} and overnight incubation at 16°C. An aliquot of cells was removed for analys is of the “total expression” of N-GTPase protein and compared to cells prior to IPTG induction. Remaining cells were harvested by centrifugation at 30 min at 2,000×*g* and the supernatant discarded. The cell pellet was resuspended in 0.5 ml B-PER reagent (ThermoFisher) containing 1 mM PMSF and 10ug/mL DNase I (bovine pancreas, Sigma) and incubated for 30 min at 4°C. Lysates were clarified by centrifugation at 16,900×*g* for 15 min at 4°C, and an aliquot of the supernata nt saved for the “soluble” fraction. The remaining soluble fraction was then incubated with Ni-NTA beads to capture His_6-tagged protein. To prepare the “insoluble” fraction, the pellet was resuspended in 0.5 ml 6 M Urea, heated at 95°C for 15 min, centrifuged at 16,900×*g* for 15 min to remove debris, and the supernatant saved. All proteins were resolved by 15% SDS PAGE and visualized by staining with Coomassie Brilliant Blue R 250 stain.

Crystallization and structure determination—Crystallization trials of tag-free p190RhoGAP-A N-GTPase protein (residues 1-266) at 10 mg/ml were performed by sparse matrix (NeXtal DWBlock JCSG+ and Classics Suites, Qiagen) and grid screening (NeXtal DWBlock PEGs and AmSO4 Suites, Qiagen) using a TTP Labtech Mosquito in sitting drop vapor diffusion plates at room temperature with a 1:1 (v/v) ratio of protein to reservoir solution with final drop volume of 0.5 μl. Single small crystals were obtained after several weeks in drops derived from condition D10 of the PEGs Suite which contains 25% (w/v) PEG 8000, 100 mM Tris HCl pH 8.5. Crystals were harvested and washed in reservoir solution supplemented with cryo-preservative (15% ethylene glycol), and flash-cooled in liquid nitrogen. Eight sets of diffraction data were collected from a single crystal at Northeastern Collaborative Access Team (NE-CAT) Beamline 24-ID-E at Argonne National Laboratory Advanced Photon Source, processed and integrated separately in XDS (Kabsch, 2010), then scaled together in XDS with XSCALE to improve completeness and resolution

to 2.8 Å. Data were processed in space group $P2_12_12_1$. Matthews probability calculator predicted two copies of N-GTPase in the asymmetric unit. A partial molecular replacement solution using the coordinates of H-Ras protein (PDB ID: 5P21 (Pai et al., 1990)) was obtained in Phenix Phaser (Adams et al., 2010; McCoy et al., 2007) for one copy with a translation function Z-score (TFZ) of 7.5, but placement of the second copy was difficult. Ultimately, a molecular replacement solution was found in Phenix Phaser using the unpublished p190-A N-GTPase coordinates from Structural Genomics Consortium (PDB ID: 3C5H) lacking nucleotide and divalent cation as a search model, with a translation function z-score (TFZ) of 27.6 for two copies. Search model bias was mitigated by autobuilding and simulated annealing. Manual model building was performed in coot (Emsley et al., 2010) and refinement in Phenix (Afonine et al., 2012). GTP and Mg^{2+} were modelled into unbiased positive F_{obs} - F_{calc} electron density maps after the N-GTPase molecules were built and refined for multiple rounds. Upon modeling and refinement of GTP and Mg^{2+}, all three phosphates of GTP remain in good electron density (Fig. 4b) and have near-equivalent temperature factors (phosphorous atoms α:69, β:64, γ:70), strongly suggesting that a triphosphate nucleotide, rather than a diphosphate, is bound to N-GTPase in the crystal structure. The final model contains two copies of N-GTPase with GTP/Mg^{2+} bound. All crystallography software was compiled by SBGrid (Morin et al., 2013). Structure superposition was performed by Dali server (Holm and Rosenstrom, 2010), interface and crystal packing analysis by Pisa (Krissinel and Henrick, 2007), GTP binding analysis by PDBSUM (Laskowski et al., 1997). All structure figures were generated in CCP4mg (McNicholas et al., 2011).

Strong anion exchange analysis of nucleotide—Purified p190RhoGAP N-GTPase and Rac1 proteins (at approximately 0.5 mM) were heat denatured at 95°C in the presence of 5 mM EDTA, and the precipitated protein removed from solution by centrifugation at 16900 x g at 4°C for 15 min. The supernatant containing nucleotide was then diluted tenfold in Buffer A (20 mM Tris pH 7.5) for a final NaCl concentration to 15 mM. The sample was bound to a Mono Q Strong Anion Exchange Column (GE Healthcare) on an AKTA Purifier FPLC (GE Healthcare), and the nucleotide eluted with a gradient of Buffer B (20 mM Tris pH 7.5 with 1 M NaCl) from 0 to 100% over 20 column volumes. The elution profile of nucleotide was monitored at absorbance 254 nm and the area under the peak was calculated (Unicorn software version 5.31, GE Healthcare). The elution profiles of the nucleotides alone were first calibrated by loading GTP and GDP individually on the MonoQ and eluted under identical gradient conditions. GTP elutes at 34.5% B, whereas GDP elutes at 29.1% B; the two peaks are easily distinguishable. Lyophilized nucleotides at purity >95% were purchased by Sigma, Thermo, and dissolved in 20 mM Tris pH 7.4. Concentrations were verified by A260 using extinction coefficient of GTP at 254nm (13,700 m^{-1} cm^{-1}). For GTP hydrolysis measurements, wild-type Rac1 (at 0.5 mM) was supplemented with tenfold molar excess of GTP and $MgCl_2$ (5 mM each) and incubated at room temperature. The reaction was measured at time zero (immediately after GTP and Mg addition) and at 24 hrs. Similarly, N-GTPase at 0.5 mM (which purifies in its GTP bound form) was incubated at room temperature with 5 mM $MgCl_2$, and samples taken at time zero and 24 hr. These methods were adapted from previous studies (Ogita et al., 2015; Zavialov et al., 2001).

Thermal shift assays—Thermal shift assays were performed as described previously (Stiegler and Boggon, 2017) and ((Murphy et al., 2014). Protein at 5μM in 20 mM Tris pH 7.4, 150 mM NaCl was mixed with SYPRO Orange (ThermoFisher; stock solution at 5000×) at a final concentration of 5× in the presence or absence of divalent cation or guanine nucleotide at varying concentrations, in a total reaction volume of 25 μl. A Bio-Rad CFX Connect Real-time PCR machine with FAM filters was used to collect data. The mixture was pre-equilibrated to 4°C for 5 min, followed by thermal ramping of 1°C per min from 4 to 95°C, with fluores cence measurements taken after each 1 °C increment. Fluorescence signal was normalized and plotted as a function of temperature, and data were fit to a sigmoidal curve in Prism 7 (Graphpad) with R^2 values of >0.99. The midway inflection point of the curve represents the melting temperature (T_m). Points after the fluorescence maximum were excluded from fitting. Changes in the melting temperature (ΔT_m) compared to the buffer-only control curve were calculated for each ligand pair and reported as the difference in T_m. The mean and SD of four experiments was determined.

Nucleotide exchange assays—MANT-GTP was purchased from Thermofisher. Binding of 0.5 μM MANT-GTPγS to 1–2 μM purified protein was measured at room temperature in buffer containing 20 mM Tris pH 7.5, 50 mM NaCl, plus or minus 1-10 mM $MgCl_2$ or 2-20 mM EDTA as indicated, in 100 μl reaction volumes in a black-bottomed microplate. Fluorescence data were collected on a BioTek Synergy 2 multi-mode reader with excitation/emission filters of 360/40 and 450/50, respectively. A time course of binding was carried out with fluorescence measurements taken every 30 s for 30 min, with protein added to nucleotide after 3 baseline measurements (which were averaged as signal at time zero). In each experiment, the fluorescence signal was normalized to time zero. Purified H-Ras G12V was used as a positive control.

QUANTIFICATION AND STATISTICAL ANALYSIS

For quantitation of bound nucleotide by anion exchange chromatography in Figure 4e, the elution profile of nucleotide was monitored at absorbance 254 nm and the area under the peak was calculated by Unicorn software version 5.31 (GE Healthcare). A scatter dot plot is used to show each data point, with the bar graph indicating the mean of each column. Error bars indicate standard deviation. P-values are indicated as determined in Prism 7 by a pairwise t-test, two-tailed (n=5 for N-GTPase and n=3 for Rac1). For differential scanning fluorimetry determination of melting temperature in Figure 5h-i, the fluorescent signal of SYPRO orange dye was monitored over time and recorded in a Bio-Rad CFX Connect Real-time PCR machine with FAM filters. Data were transferred to GraphPad Prism 7, where fluorescent data for each sample was first normalized and then plotted against time. Curve fitting was performed in Prism 7 using nonlinear regression analysis (using least squares fit) with a sigmoidal dose-response (variable slope) equation where the bottom and top values are constrained to 0 and 100, respectively. For each curve used, the goodness of fit is at least R = 0.99 as determined in Prism. The temperature at which the normalized fluorescence is 50 corresponds to the melting temperature. The scatter dot plot in Figure 5i shows each data point, while the bar graph indicates the mean of each protein with error bars as standard deviation. n=4 for each protein. P-values for mutants versus wild-type are indicated above

the bar graph as determined by Ordinary one-way ANOVA (no pairing) analysis corrected for multiple comparisons by Tukey's test with a single pooled variance in Prism 7.

DATA AND SOFTWARE AVAILABILITY

Coordinates and structure factors have been deposited in the Protein Data Bank under accession code, 6D4G. X-ray diffraction images are available online at SBGrid Data Bank: doi:10.15785/SBGRID/575.

Supplementary Material

Refer to Web version on PubMed Central for supplementary material.

Acknowledgements

Anthony Koleske is thanked for helpful discussions and for providing p190RhoGAP-A cDNA. Anatoly Kiyatkin and Mark Lemmon are thanked for use of the BioTek Synergy 2 plate reader for the MANT assays. Leena Kuruvilla is thanked for assistance with the thermal shift assays. David Calderwood is thanked for the H-Ras cDNA. Albert Chan is thanked for technical help with XDS. ByungHak Ha is thanked for technical input. Staff at beamline 24-ID-E (NE-CAT-E) at the Advanced Photon Source, Argonne National Laboratory are thanked. This work is based upon research conducted at the Northeastern Collaborative Access Team beamlines, which are funded by National Institutes of Health grant P41GM103403. This research used resources of the Advanced Photon Source, a U.S. Department of Energy (DOE) Office of Science User Facility operated for the DOE Office of Science by Argonne National Laboratory under Contract No. DE-AC02-06CH11357. National Institutes of Health grants R01NS085078, R01GM102262, S10OD018007 funded the research.

References

Adams PD, Afonine PV, Bunkoczi G, Chen VB, Davis IW, Echols N, Headd JJ, Hung LW, Kapral GJ, Grosse-Kunstleve RW, et al. (2010). PHENIX: a comprehensive Python-based system for macromolecular structure solution. Acta crystallographica Section D, Biological crystallography 66, 213–221. [PubMed: 20124702]

Afonine PV, Grosse-Kunstleve RW, Echols N, Headd JJ, Moriarty NW, Mustyakimov M, Terwilliger TC, Urzhumtsev A, Zwart PH, and Adams PD (2012). Towards automated crystallographic structure refinement with phenix.refine. Acta crystallogr D 68, 352–367. [PubMed: 22505256]

Ahmadian MR, Stege P, Scheffzek K, and Wittinghofer A (1997). Confirmation of the arginine-finger hypothesis for the GAP-stimulated GTP-hydrolysis reaction of Ras. Nat Struct Biol 4, 686–689. [PubMed: 9302992]

Amin E, Jaiswal M, Derewenda U, Reis K, Nouri K, Koessmeier KT, Aspenstrom P, Somlyo AV, Dvorsky R, and Ahmadian MR (2016). Deciphering the Molecular and Functional Basis of RHOGAP Family Proteins: A SYSTEMATIC APPROACH TOWARD SELECTIVE INACTIVATION OF RHO FAMILY PROTEINS. J Biol Chem 291, 20353–20371. [PubMed: 27481945]

Arthur WT, and Burridge K (2001). RhoA inactivation by p190RhoGAP regulates cell spreading and migration by promoting membrane protrusion and polarity. Mol Biol Cell 12, 2711–2720. [PubMed: 11553710]

Artim SC, Mendrola JM, and Lemmon MA (2012). Assessing the range of kinase autoinhibition mechanisms in the insulin receptor family. Biochem J 448, 213–220. [PubMed: 22992069]

Bandaranayake RM, Ungureanu D, Shan Y, Shaw DE, Silvennoinen O, and Hubbard SR (2012). Crystal structures of the JAK2 pseudokinase domain and the pathogenic mutant V617F. Nature structural & molecular biology 19, 754–759.

Basilico F, Maffini S, Weir JR, Prumbaum D, Rojas AM, Zimniak T, De Antoni A, Jeganathan S, Voss B, van Gerwen S, et al. (2014). The pseudo GTPase CENP-M drives human kinetochore assembly. Elife 3, e02978. [PubMed: 25006165]

Blaum BS, Mazzotta S, Noldeke ER, Halter T, Madlung J, Kemmerling B, and Stehle T (2014). Structure of the pseudokinase domain of BIR2, a regulator of BAK1-mediated immune signaling in Arabidopsis. J Struct Biol 186, 112–121. [PubMed: 24556575]

Boudeau J, Miranda-Saavedra D, Barton GJ, and Alessi DR (2006). Emerging roles of pseudokinases. Trends Cell Biol 16, 443–452. [PubMed: 16879967]

Bourne HR, Sanders DA, and McCormick F (1991). The GTPase superfamily: conserved structure and molecular mechanism. Nature 349, 117–127. [PubMed: 1898771]

Brennan DF, Dar AC, Hertz NT, Chao WC, Burlingame AL, Shokat KM, and Barford D (2011). A Raf-induced allosteric transition of KSR stimulates phosphorylation of MEK. Nature 472, 366–369. [PubMed: 21441910]

Burbelo PD, Miyamoto S, Utani A, Brill S, Yamada KM, Hall A, and Yamada Y (1995). p190-B, a new member of the Rho GAP family, and Rho are induced to cluster after integrin cross-linking. J Biol Chem 270, 30919–30926. [PubMed: 8537347]

Chang JH, Gill S, Settleman J, and Parsons SJ (1995). c-Src regulates the simultaneous rearrangement of actin cytoskeleton, p190RhoGAP, and p120RasGAP following epidermal growth factor stimulation. J Cell Biol 130, 355–368. [PubMed: 7542246]

Davis MJ, Ha BH, Holman EC, Halaban R, Schlessinger J, and Boggon TJ (2013). RAC1P29S is a spontaneously activating cancer-associated GTPase. Proc Natl Acad Sci U S A 110, 912–917. [PubMed: 23284172]

Der CJ, Finkel T, and Cooper GM (1986). Biological and biochemical properties of human rasH genes mutated at codon 61. Cell 44, 167–176. [PubMed: 3510078]

Dever TE, Glynias MJ, and Merrick WC (1987). GTP-binding domain: three consensus sequence elements with distinct spacing. Proc Natl Acad Sci U S A 84, 1814–1818. [PubMed: 3104905]

Emsley P, Lohkamp B, Scott WG, and Cowtan K (2010). Features and development of Coot. Acta crystallogr D 66, 486–501. [PubMed: 20383002]

Eyers PA, and Murphy JM (2016). The evolving world of pseudoenzymes: proteins, prejudice and zombies. BMC biology 14, 98. [PubMed: 27835992]

Fetics SK, Guterres H, Kearney BM, Buhrman G, Ma B, Nussinov R, and Mattos C (2015). Allosteric effects of the oncogenic RasQ61L mutant on Raf-RBD. Structure 23, 505–516. [PubMed: 25684575]

Foster R, Hu KQ, Lu Y, Nolan KM, Thissen J, and Settleman J (1996). Identification of a novel human Rho protein with unusual properties: GTPase deficiency and in vivo farnesylation. Mol Cell Biol 16, 2689–2699. [PubMed: 8649376]

Foster R, Hu KQ, Shaywitz DA, and Settleman J (1994). p190 RhoGAP, the major RasGAP-associated protein, binds GTP directly. Mol Cell Biol 14, 7173–7181. [PubMed: 7935432]

Fukuda K, Gupta S, Chen K, Wu C, and Qin J (2009). The pseudoactive site of ILK is essential for its binding to alpha-Parvin and localization to focal adhesions. Mol Cell 36, 819–830. [PubMed: 20005845]

Ha BH, and Boggon TJ (2018). The crystal structure of pseudokinase PEAK1 (Sugen kinase 269) reveals an unusual catalytic cleft and a novel mode of kinase fold dimerization. J Biol Chem 293, 1642–1650. [PubMed: 29212708]

Hall A, and Self AJ (1986). The effect of Mg2+ on the guanine nucleotide exchange rate of p21N-ras. J Biol Chem 261, 10963–10965. [PubMed: 3525557]

Holm L, and Rosenstrom P (2010). Dali server: conservation mapping in 3D. Nucleic acids research 38, W545–549. [PubMed: 20457744]

Jaffe AB, and Hall A (2005). Rho GTPases: biochemistry and biology. Annual review of cell and developmental biology 21, 247–269.

Kabsch W (2010). Xds. Acta crystallogr D 66, 125–132. [PubMed: 20124692]

Krissinel E, and Henrick K (2007). Inference of macromolecular assemblies from crystalline state. Journal of molecular biology 372, 774–797. [PubMed: 17681537]

Laskowski RA, Hutchinson EG, Michie AD, Wallace AC, Jones ML, and Thornton JM (1997). PDBsum: a Web-based database of summaries and analyses of all PDB structures. Trends in biochemical sciences 22, 488–490. [PubMed: 9433130]

LeClerc S, Palaniswami R, Xie BX, and Govindan MV (1991). Molecular cloning and characterization of a factor that binds the human glucocorticoid receptor gene and represses its expression. J Biol Chem 266, 17333–17340. [PubMed: 1894621]

Lecointre C, Simon V, Kerneur C, Allemand F, Fournet A, Montarras I, Pons JL, Gelin M, Brignatz C, Urbach S, et al. (2018). Dimerization of the Pragmin Pseudo-Kinase Regulates Protein Tyrosine Phosphorylation. Structure 26, 545–554. e544. [PubMed: 29503074]

Lin R, Bagrodia S, Cerione R, and Manor D (1997). A novel Cdc42Hs mutant induces cellular transformation. Curr Biol 7, 794–797. [PubMed: 9368762]

Manning G, Whyte DB, Martinez R, Hunter T, and Sudarsanam S (2002). The protein kinase complement of the human genome. Science 298, 1912–1934. [PubMed: 12471243]

McCoy AJ, Grosse-Kunstleve RW, Adams PD, Winn MD, Storoni LC, and Read RJ (2007). Phaser crystallographic software. J Appl Crystallogr 40, 658–674. [PubMed: 19461840]

McNicholas S, Potterton E, Wilson KS, and Noble ME (2011). Presenting your structures: the CCP4mg molecular-graphics software. Acta crystallogr D Biol Crystallogr 67, 386–394. [PubMed: 21460457]

Min X, Lee BH, Cobb MH, and Goldsmith EJ (2004). Crystal structure of the kinase domain of WNK1, a kinase that causes a hereditary form of hypertension. Structure 12, 1303–1311. [PubMed: 15242606]

Min X, Ungureanu D, Maxwell S, Hammaren H, Thibault S, Hillert EK, Ayres M, Greenfield B, Eksterowicz J, Gabel C, et al. (2015). Structural and Functional Characterization of the JH2 Pseudokinase Domain of JAK Family Tyrosine Kinase 2 (TYK2). J Biol Chem 290, 27261–27270. [PubMed: 26359499]

Morin A, Eisenbraun B, Key J, Sanschagrin PC, Timony MA, Ottaviano M, and Sliz P (2013). Collaboration gets the most out of software. Elife 2.

Mukherjee K, Sharma M, Urlaub H, Bourenkov GP, Jahn R, Sudhof TC, and Wahl MC (2008). CASK Functions as a Mg2+-independent neurexin kinase. Cell 133, 328–339. [PubMed: 18423203]

Murphy JM, Farhan H, and Eyers PA (2017a). Bio-Zombie: the rise of pseudoenzymes in biology. Biochem Soc Trans 45, 537–544. [PubMed: 28408493]

Murphy JM, Mace PD, and Eyers PA (2017b). Live and let die: insights into pseudoenzyme mechanisms from structure. Current opinion in structural biology 47, 95–104. [PubMed: 28787627]

Murphy JM, Zhang Q, Young SN, Reese ML, Bailey FP, Eyers PA, Ungureanu D, Hammaren H, Silvennoinen O, Varghese LN, et al. (2014). A robust methodology to subclassify pseudokinases based on their nucleotide-binding properties. Biochem J 457, 323–334. [PubMed: 24107129]

Ogita Y, Egami S, Ebihara A, Ueda N, Katada T, and Kontani K (2015). Di-Ras2 Protein Forms a Complex with SmgGDS Protein in Brain Cytosol in Order to Be in a Low Affinity State for Guanine Nucleotides. J Biol Chem 290, 20245–20256. [PubMed: 26149690]

Pai EF, Krengel U, Petsko GA, Goody RS, Kabsch W, and Wittinghofer A (1990). Refined crystal structure of the triphosphate conformation of H-ras p21 at 1.35 A resolution: implications for the mechanism of GTP hydrolysis. EMBO J 9, 2351–2359. [PubMed: 2196171]

Patel O, Griffin MDW, Panjikar S, Dai W, Ma X, Chan H, Zheng C, Kropp A, Murphy JM, Daly RJ, et al. (2017). Structure of SgK223 pseudokinase reveals novel mechanisms of homotypic and heterotypic association. Nature communications 8, 1157.

Pils B, and Schultz J (2004). Inactive enzyme-homologues find new function in regulatory processes. J Mol Biol 340, 399–404. [PubMed: 15210342]

Ridley AJ, Self AJ, Kasmi F, Paterson HF, Hall A, Marshall CJ, and Ellis C (1993). rho family GTPase activating proteins p190, bcr and rhoGAP show distinct specificities in vitro and in vivo. EMBO J 12, 5151–5160. [PubMed: 8262058]

Romani AM (2011). Cellular magnesium homeostasis. Arch Biochem Biophys 512, 1–23. [PubMed: 21640700]

Roof RW, Dukes BD, Chang JH, and Parsons SJ (2000). Phosphorylation of the p190 RhoGAP N-terminal domain by c-Src results in a loss of GTP binding activity. FEBS Lett 472, 117–121. [PubMed: 10781817]

Scheeff ED, Eswaran J, Bunkoczi G, Knapp S, and Manning G (2009). Structure of the Pseudokinase VRK3 Reveals a Degraded Catalytic Site, a Highly Conserved Kinase Fold, and a Putative Regulatory Binding Site. Structure 17, 128–138. [PubMed: 19141289]

Scheffzek K, Ahmadian MR, Kabsch W, Wiesmuller L, Lautwein A, Schmitz F, and Wittinghofer A (1997). The Ras-RasGAP complex: structural basis for GTPase activation and its loss in oncogenic Ras mutants. Science 277, 333–338. [PubMed: 9219684]

Schroeder CM, Ostrem JM, Hertz NT, and Vale RD (2014). A Ras-like domain in the light intermediate chain bridges the dynein motor to a cargo-binding region. Elife 3, e03351. [PubMed: 25272277]

Settleman J, Narasimhan V, Foster LC, and Weinberg RA (1992). Molecular cloning of cDNAs encoding the GAP-associated protein p190: implications for a signaling pathway from ras to the nucleus. Cell 69, 539–549. [PubMed: 1581965]

Shi F, Telesco SE, Liu Y, Radhakrishnan R, and Lemmon MA (2010). ErbB3/HER3 intracellular domain is competent to bind ATP and catalyze autophosphorylation. Proc Natl Acad Sci U S A 107, 7692–7697. [PubMed: 20351256]

Sievers F, Wilm A, Dineen D, Gibson TJ, Karplus K, Li WZ, Lopez R, McWilliam H, Remmert M, Soding J, et al. (2011). Fast, scalable generation of high-quality protein multiple sequence alignments using Clustal Omega. Molecular systems biology 7.

Smith SJ, and Rittinger K (2002). Preparation of GTPases for structural and biophysical analysis. Methods in molecular biology 189, 13–24. [PubMed: 12094582]

Snyder JT, Worthylake DK, Rossman KL, Betts L, Pruitt WM, Siderovski DP, Der CJ, and Sondek J (2002). Structural basis for the selective activation of Rho GTPases by Dbl exchange factors. Nat Struct Biol 9, 468–475. [PubMed: 12006984]

Soundararajan M, Yang X, Elkins JM, Sobott F, and Doyle DA (2007). The centaurin gamma-1 GTPase-like domain functions as an NTPase. Biochem J 401, 679–688. [PubMed: 17037982]

Splingard A, Menetrey J, Perderiset M, Cicolari J, Regazzoni K, Hamoudi F, Cabanie L, El Marjou A, Wells A, Houdusse A, et al. (2007). Biochemical and structural characterization of the gem GTPase. J Biol Chem 282, 1905–1915. [PubMed: 17107948]

Stiegler AL, and Boggon TJ (2017). p190RhoGAP proteins contain pseudoGTPase domains. Nature communications 8, 506.

Tatsis N, Lannigan DA, and Macara IG (1998). The function of the p190 Rho GTPase-activating protein is controlled by its N-terminal GTP binding domain. J Biol Chem 273, 34631–34638. [PubMed: 9852136]

Toms AV, Deshpande A, McNally R, Jeong Y, Rogers JM, Kim CU, Gruner SM, Ficarro SB, Marto JA, Sattler M, et al. (2013). Structure of a pseudokinase-domain switch that controls oncogenic activation of Jak kinases. Nature structural & molecular biology 20, 1221–1223.

Tong LA, de Vos AM, Milburn MV, and Kim SH (1991). Crystal structures at 2.2 A resolution of the catalytic domains of normal ras protein and an oncogenic mutant complexed with GDP. J Mol Biol 217, 503–516. [PubMed: 1899707]

Vetter IR, and Wittinghofer A (2001). The guanine nucleotide-binding switch in three dimensions. Science 294, 1299–1304. [PubMed: 11701921]

Vincent S, and Settleman J (1999). Inhibition of RhoGAP activity is sufficient for the induction of Rho-mediated actin reorganization. Eur J Cell Biol 78, 539–548. [PubMed: 10494860]

Wallace AC, Laskowski RA, and Thornton JM (1995). LIGPLOT: a program to generate schematic diagrams of protein-ligand interactions. Protein engineering 8, 127–134. [PubMed: 7630882]

Wennerberg K, Rossman KL, and Der CJ (2005). The Ras superfamily at a glance. J Cell Sci 118, 843–846. [PubMed: 15731001]

Xia C, Ma W, Stafford LJ, Liu C, Gong L, Martin JF, and Liu M (2003). GGAPs, a new family of bifunctional GTP-binding and GTPase-activating proteins. Mol Cell Biol 23, 2476–2488. [PubMed: 12640130]

Zavialov AV, Buckingham RH, and Ehrenberg M (2001). A posttermination ribosomal complex is the guanine nucleotide exchange factor for peptide release factor RF3. Cell 107, 115–124. [PubMed: 11595190]

Zeqiraj E, Filippi BM, Goldie S, Navratilova I, Boudeau J, Deak M, Alessi DR, and van Aalten DM (2009). ATP and MO25alpha regulate the conformational state of the STRADalpha pseudokinase and activation of the LKB1 tumour suppressor. PLoS biology 7, e1000126. [PubMed: 19513107]

Zhang B, Zhang Y, Wang Z, and Zheng Y (2000). The role of Mg2+ cofactor in the guanine nucleotide exchange and GTP hydrolysis reactions of Rho family GTP-binding proteins. J Biol Chem 275, 25299–25307. [PubMed: 10843989]

Highlights:

- p190RhoGAP N-GTPase domain is a pseudoGTPase
- The crystal structure of N-GTPase from p190RhoGAP-A is presented
- p190RhoGAP N-GTPase binds constitutively to GTP but lacks GTPase activity
- Six unique insert sequences provide a potential protein-protein interaction surface

Stiegler et al. present the crystal structure of the p190RhoGAP N-terminal GTPase and provide biochemical evidence that it binds GTP constitutively yet lacks hydrolysis activity. Thus, this domain can be classified as a pseudoGTPase.

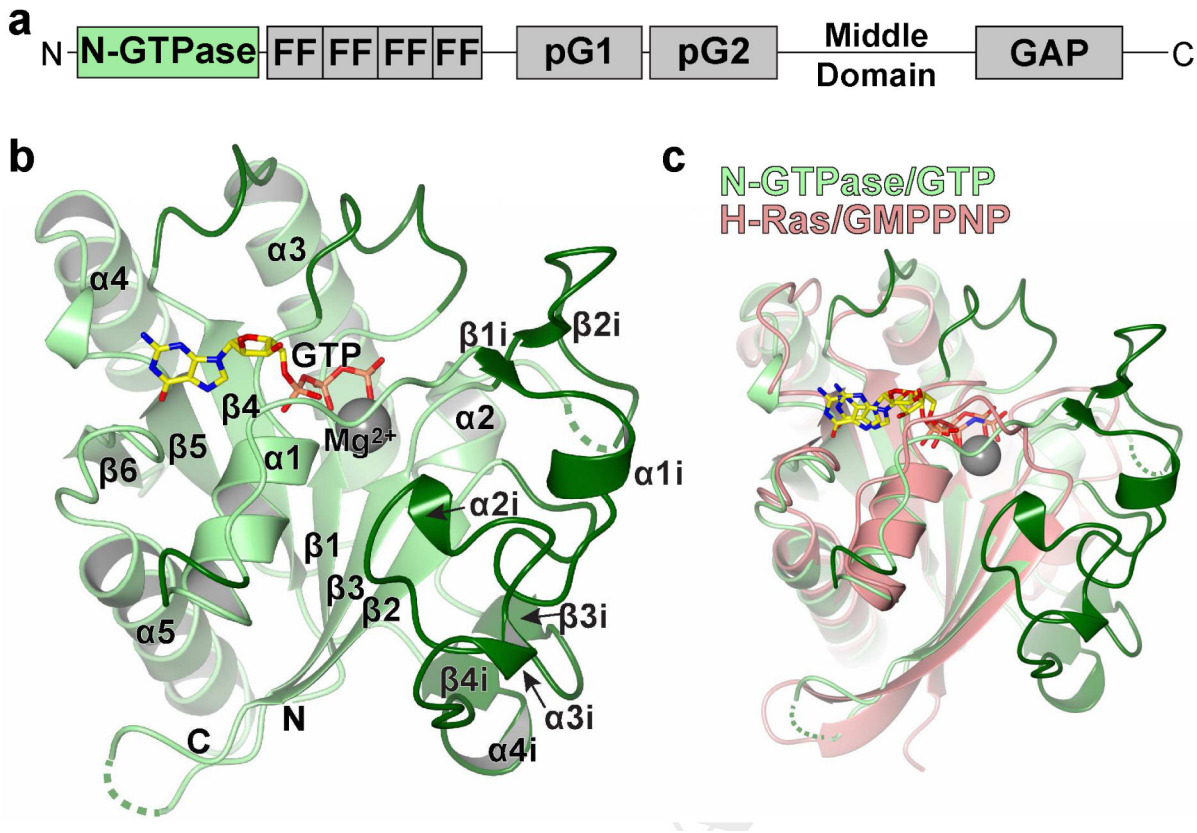

Figure 1. Crystal structure of p190RhoGAP-A N-GTPase domain.

a) Domain assignment for p190RhoGAP protein. **b)** Ribbon diagram of the structure of p190RhoGAP N-GTPase domain (copy A). Secondary structure elements, GTP and Mg^{2+} are labeled, and the inserts unique to p190RhoGAP are colored in dark green. **c)** Ribbon diagram of the structural superposition of N-GTPase (green) with H-Ras (salmon) bound to nonhydrolyzable GTP analogue, GMP-PNP (PDB ID: 5P21) (Pai et al., 1990). Superposition performed by Dali (Holm and Rosenstrom, 2010).

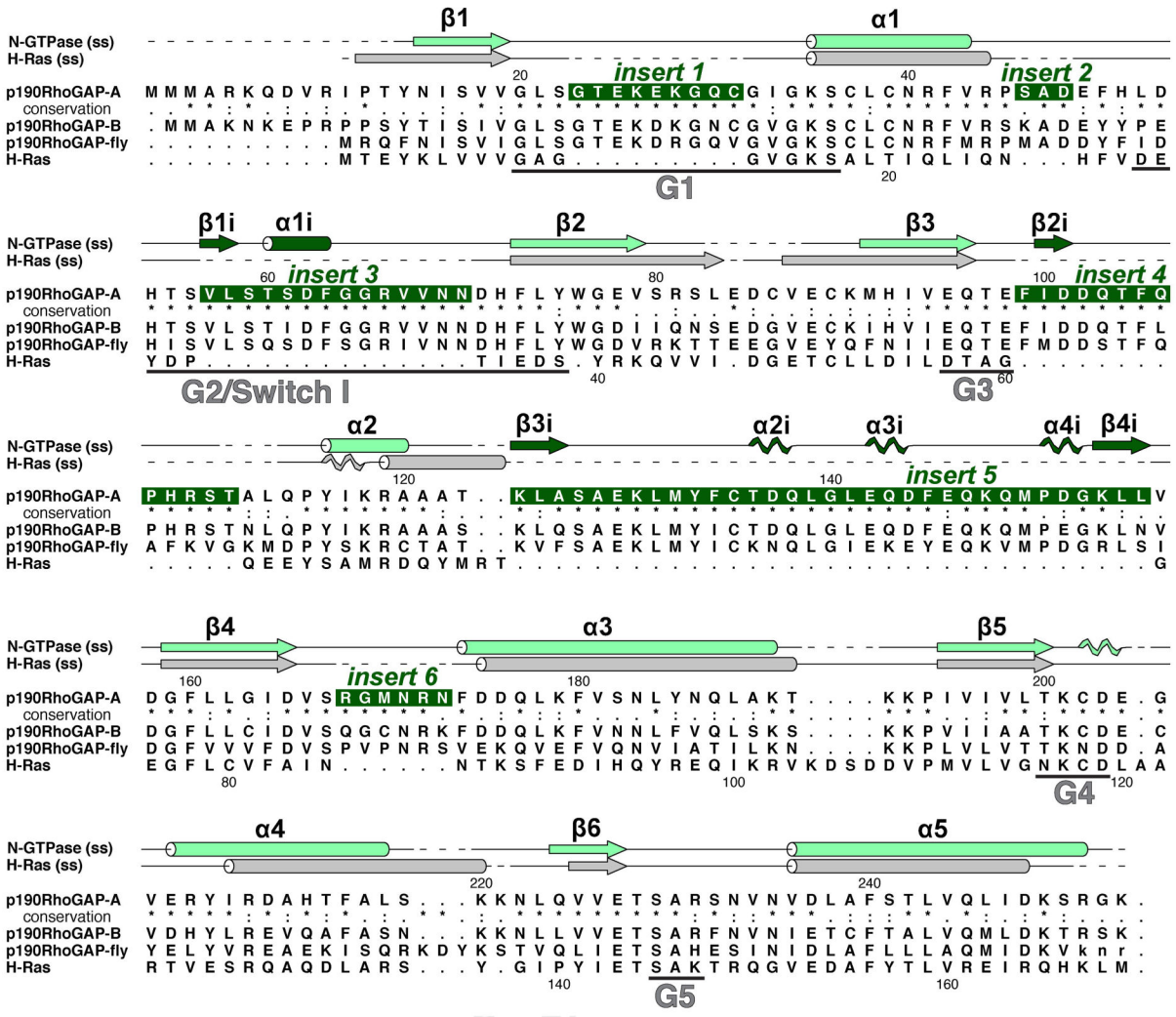

Figure 2. Sequence features and conservation.

Structure-based sequence alignment of N-GTPase with H-Ras, with secondary structure elements drawn and labeled above the sequences. The location of the consensus GTPase G-motifs (underlined) and N-GTPase inserts (dark green) are indicated. The conservation p190RhoGAP-A (ARHGAP35) protein sequence from 77 species is shown; (*) identical, (:) strongly similar, (.) weakly similar, as determined by ClustalO (Sievers et al., 2011). Aligned sequences of p190RhoGAP-B (ARHGAP5) (72% identical) and the single p190RhoGAP gene from fly (54% identical) are also shown.

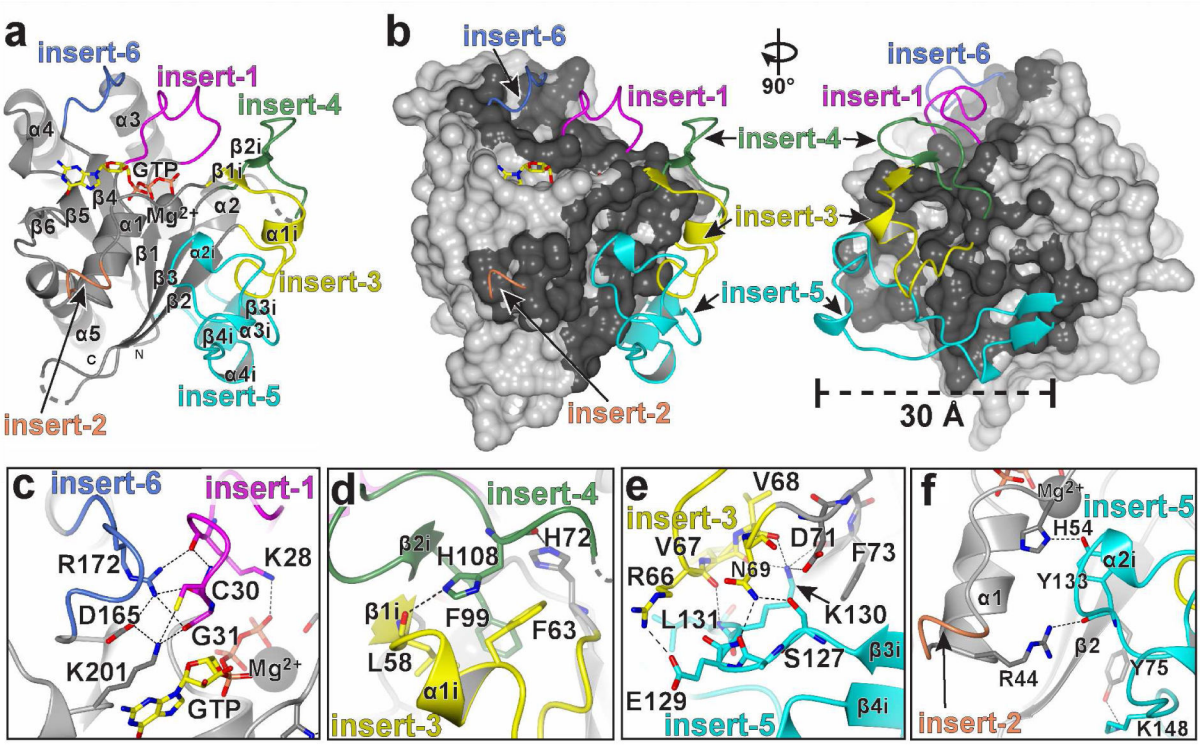

Figure 3. The p190 N-GTPase domain contains unique inserts that extend the GTPase domain.

a) Overall structure of N-GTPase with inserts colored and labeled. **b)** Core GTPase domain structure is shown in surface representation, with insert ribbons colored as in part a. Regions of the core GTPase domain that are buried by the inserts are colored dark grey. Two views related by a 90 degree rotation about the y-axis are shown. **c-f)** Specific interactions of the insert residues with each other and with the GTPase core. Inserts are colored as in part a.

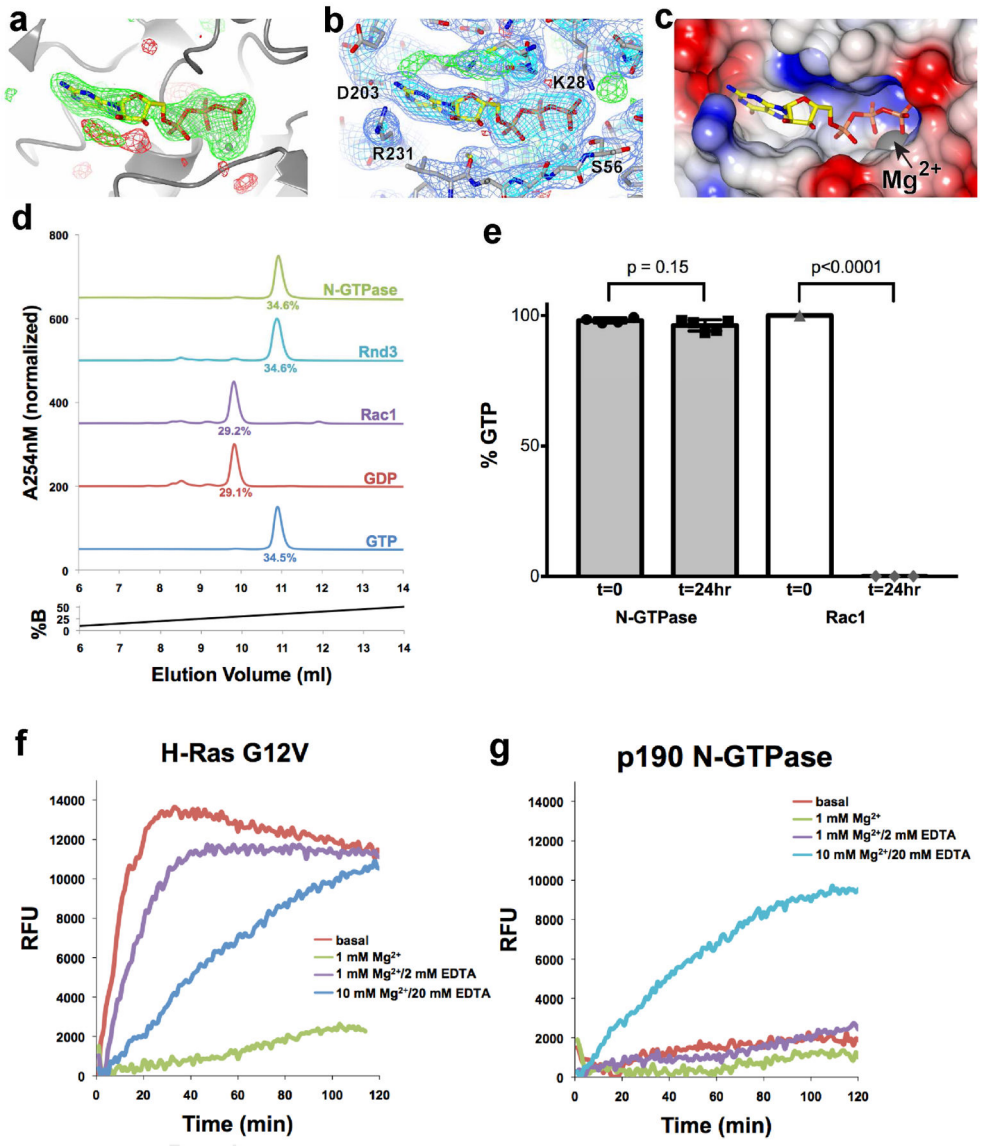

Figure. 4. The N-GTPase catalytic cleft binds both GTP and Mg^{2+} but is enzymatically inactive.

a) Unbiased difference electron density map ($F_{obs} - F_{calc}$) calculated before GTP and Mg^{2+} model building, with final refined GTP and Mg^{2+} positions shown. Map is contoured at +3 σ (*green*) and −3 σ (*red*). **b)** Final refined $2F_{obs} - F_{calc}$ map contoured at 1 σ (*blue*) and 3 σ (*cyan*), and final $F_o - F_c$ electron density map contoured at +3 σ (*green*) and −3 σ (*red*). **c)** Surface electrostatic potential of N-GTPase at the GTP/Mg^{2+} binding site. **d)** Strong anion exchange chromatography shows that N-GTPase is bound predominantly to GTP. Protein samples were denatured and precipitated, and the remaining nucleotide in solution was loaded onto a strong anion exchange column. Chromatography traces at absorbance of 254 nm is shown for purified N-GTPase (green), Rnd3 (cyan), and Rac1 wild-type (purple). The elution profiles of GDP (burgundy) and GTP (blue) were calibrated using nucleotides alone (commercially purchased). The absorbance values are normalized and offset. **e)** N-GTPase lacks hydrolysis activity *in vitro*. Strong Anion exchange chromatography was used to

measure the relative level of GTP remaining after incubation of 0.5 mM protein at room temperature for 24 hr in the presence of 5 mM Mg^{2+}. Rac1 was preloaded with GTP. A scatter dot plot shows each data point, with the bar graph indicating the mean of each column. P-values are indicated as determined in Prism (pairwise t-test). **f and g)** MANT-GTP exchange assays. The fluorescence of MANT-GTP is measured upon addition of H-Ras G12V (f) or p190RhoGAP N-GTPase (g) and followed over time. Curves are corrected for fluorescence of MANT-GTP alone (in absence of protein). “Basal” condition (red) indicates exchange curves without additives. Other curves are colored according to legend.

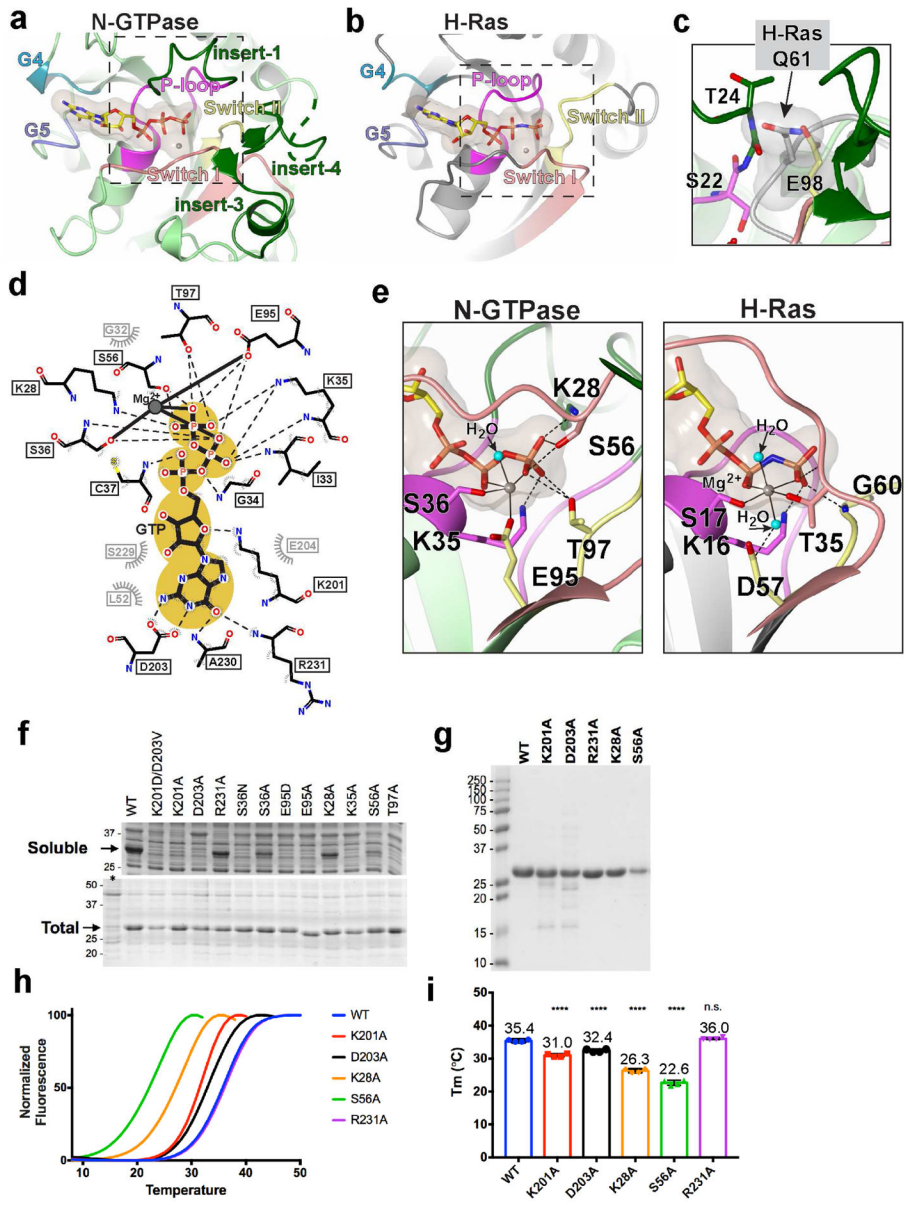

Figure 5. Analysis of GTP binding site in N-GTPase.

a) Ribbon diagram of N-GTPase structure (green) with consensus GTPase G motifs differently colored and labeled. P-loop: magenta, Switch I: pink Switch II: yellow, G4: teal, G5: purple. **b)** Ribbon diagram of H-Ras G12V (Grey) bound to GMP-PNP (PDB ID: 5P21). G motifs are colored as in part a. **c)** Zoom-in showing the superposition of H-Ras with N-GTPase and the catalytic Q61 of H-Ras (grey) sterically clashing with N-GTPase residues S22, T24, and E98. **d)** Map of N-GTPase interaction with GTP and Mg^{2+} adapted from Ligplot (Wallace et al., 1995). **e)** Detailed view of GTP gamma phosphate and Mg^{2+} binding site in N-GTPase (left) and H-Ras (right). Region shown is indicated by a dashed box in parts a and b. **f)** Solubility and total expression of N-GTPase wild-type (WT) and mutant proteins. Clarified (top) or total (bottom) lysates are resolved by SDS-PAGE and proteins visualized by Coomassie Blue staining. **g)** Final purified N-GTPase wild-type and

mutant proteins, resolved by SDS-PAGE and stained with Coomassie Blue. **h)** Thermal denaturation curves from a representative experiment of N-GTPase proteins. Fluorescence signal has been normalized in each sample. **i)** Scatter dot plot of melting temperatures calculated as the mean of four measurements for each sample (error bars indicate standard deviation) determined by fitting the melting curve to a sigmoidal model. P-values from One-way ANOVA comparisons of the melting temperatures to wild-type is indicated above each bar (****: $p < 0.0001$. n.s.: no significant difference).

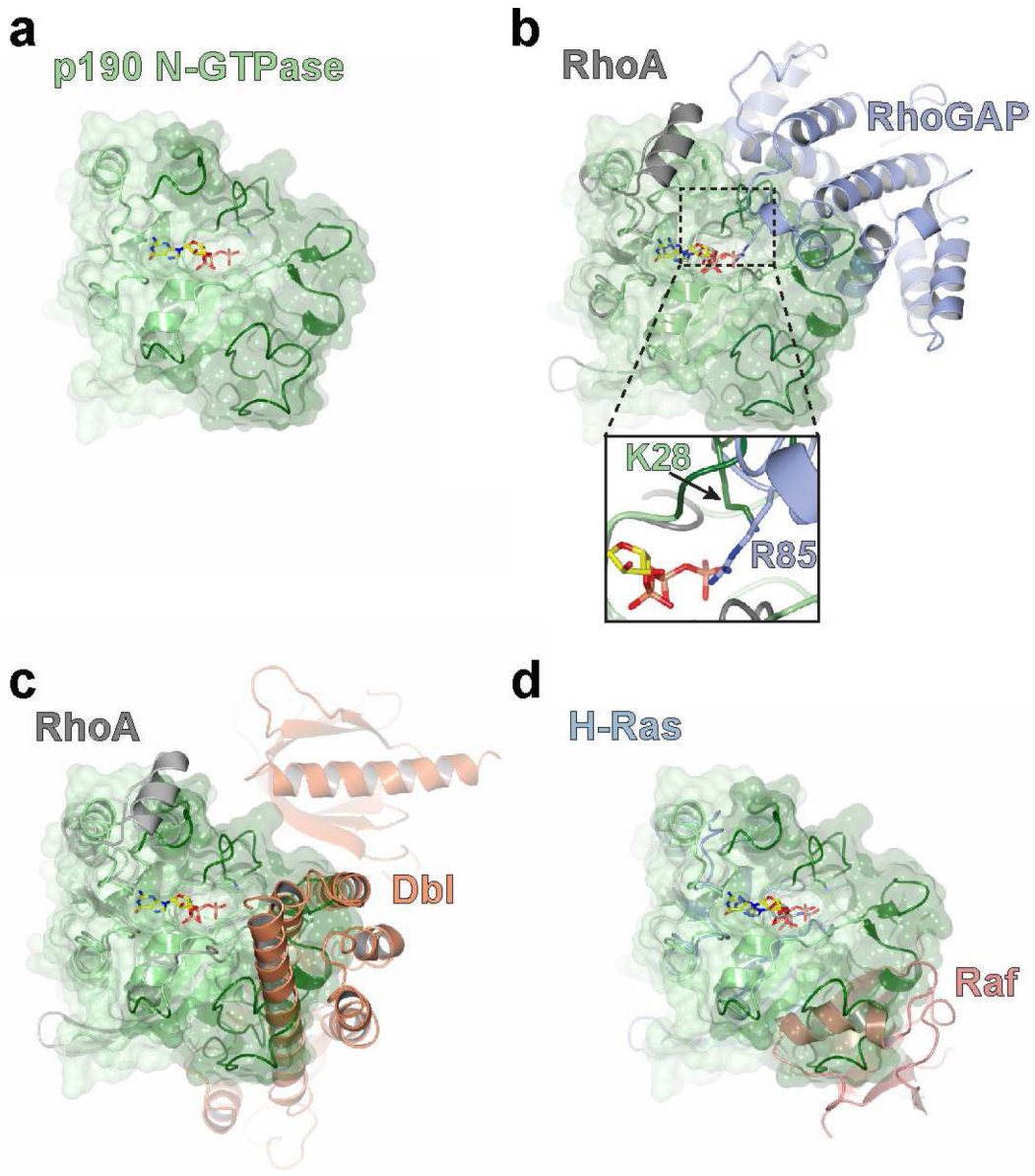

Figure 6. Binding of typical GAP, GEF, and effector molecules is sterically blocked in N-GTPase

a) Ribbon and surface representation of N-GTPase structure (green). Orientation and coloring of N-GTPase is consistent in all panels. **b)** N-GTPase superposed onto RhoA (grey) bound to GAP domain of p190RhoGAP (light purple) (PDB ID: 5IRC (Amin et al., 2016)). Inset: zoom-in of Lys-28 in N-GTPase (green) clashing with Arg-finger from GAP domain (light purple). **c)** N-GTPase superposed onto RhoA (grey) bound to GEF (Dbl domain from Dbs, light purple, PDB ID: 1LB1 (Snyder et al., 2002)). **d)** N-GTPase superposed onto H-Ras (light blue) bound to its effector Raf (pink, PDB ID:4G0N (Fetics et al., 2015)).

Table 1.

Data collection and refinement statistics. Statistics for the highest-resolution shell are shown in parentheses.

Data Collection	**PDB ID: 6D4G**
Wavelength (Å)	0.97918
Resolution range	50 - 2.8 (2.9 - 2.8)
Space group	$P2_12_12_1$
Cell dimensions a, b, c (Å)	43.7, 69.2, 154.1
Cell dimension α, β, γ (°)	90, 90, 90
Unique reflections	12096 (1194)
Multiplicity	51.6 (54.5)
Completeness (%)	99.8 (100.00)
Mean I / σ(I)	20.4 (1.9)
Wilson B-factor (Å^2)	92.7
R_{pim} (%)	2.5 (47.6)
CC½	0.99 (0.71)
CC*	1.00 (0.91)
Refinement	
Reflections used in refinement	12096 (1194)
Reflections used for R-free	605 (60)
R_{work} (%)	25.0 (31.4)
R_{free} (%)	29.0 (39.2)
CC_{work}	0.94 (0.75)
CC_{free}	0.85 (0.52)
Number of non-hydrogen atoms	3379
macromolecules	3308
ligands	66
solvent	5
Protein residues	419
R.M.S.D. (bond lengths) (Å)	0.002
R.M.S.D. (bond angles) (°)	0.67
Ramachandran plot : favored, allowed, outliers (%)	98.0, 2.0, 0
Rotamer outliers (%)	0.5
MolProbity clashscore	5.7
Average B-factor (Å^2)	129.3
macromolecules	130.2
Copy A	111.6
Copy B	151.4
ligands	88.5
solvent	69.2

Table 2.

Classification of pseudoGTPases.

Pseudoenzyme classification		Pseudokinase examples	PseudoGTPase examples
i	No nucleotide binding	VRK3 (Scheeff et al., 2009) BIR2 (Blaum et al., 2014) ROR2 (Artim et al., 2012) PEAK1 (Ha and Boggon, 2018, Pragmin (Lecointre et al., 2018; Patel et al., 2017)	p190RhoGAP pG1 and pG2 (Stiegler and Boggon, 2017) CENP-M (Basilico et al., 2014) Fungal dynein LIC (Schroeder et al., 2014)
ii	Nucleotide binding, but with no or very weak catalytic activity	ILK (Fukuda et al., 2009) TYK2 JH2 (Min et al., 2015) JAK1 JH2 (Toms et al., 2013) STRADα (Zeqiraj et al., 2009)	Rnd family (Foster et al., 1996) p190RhoGAP N-GTPase [This study]
iii	Retained catalytic activity	WNK1 (Min et al., 2004) CASK (Mukherjee et al., 2008) ErbB3 (Shi et al., 2010) JAK2 JH2 (Bandaranayake et al., 2012) KSR2 (Brennan et al., 2011)	RGK family (e.g. Gem) (Splingard et al., 2007) Centaurin gamma-1 (Soundararajan et al., 2007)

KEY RESOURCES TABLE

REAGENT or RESOURCE	SOURCE	IDENTIFIER
Bacterial and Virus Strains		
Eschericia coli (E.coli) Rosetta(DE3) competent cells	Millipore Sigma	Cat#70954
Chemicals, Peptides, and Recombinant Proteins		
GST-p190RhoGAP-A-N-GTPase$^{1-266}$ protein	This paper	NCBI NP_001258061.1
His_6-p190RhoGAP-A-N-GTPase$^{13-249}$ protein	This paper	NCBI NP_001258061.1
His_6-Rac$^{12-177}$ protein	(Davis et al., 2013)	UniProt ID: P63000
GST-Rnd3$^{19-200}$ protein	This paper	UniProt P61587
His_6-H-Ras$^{1-167}$ G12V protein	This paper	UniProt ID: P01112
Glutathione-Sepharose 4B resin	GE Healthcare	Cat#17075601
Ni-NTA Agarose resin	Qiagen	Cat#30210
HiLoad 16/600 Superdex 75 prep grade column	GE Healthcare	Cat#28989333
Mono Q 5/50 GL column	GE Healthcare	Cat#17516601
B-PER Bacterial Protein Extraction Reagent	ThermoFisher	Cat#78243
NeXtal DWBlock PEGs Suite	Qiagen	Cat#130904
NeXtal Stock PEG 8000	Qiagen	Cat#133092
NeXtal Stock TRIS-HCl pH 8.5	Qiagen	Cat#133126
GTP	Sigma	Cat#G8877
GDP	Sigma	Cat#G7127
SYPRO Orange	ThermoFisher	Cat#S6650
MANT-GTP	ThermoFisher	Cat#M12415
Critical Commercial Assays		
QuikChange Lightning Site-Directed Mutagenesis Kit	Agilent Technologies	Cat#210518
Deposited Data		
N-GTPase atomic coordinates and structure factors	This paper	PDB ID: 6D4G
X-ray diffraction images	This paper	doi:10.15785/SBGRID/575
Crystal structure of H-Ras	(Tong et al., 1991)	PDB ID: 1Q21
Crystal structure of H-Ras	(Pai et al., 1990)	PDB ID: 5P21
Crystal structure of p190RhoGAP-A GAP domain in complex with RhoA	(Amin et al., 2016)	PDB ID: 5IRC
Crystal structure of Dbl and PH domains of Dbs in complex with RhoA	(Snyder et al., 2002)	PDB ID: 1LB1
Crystal structure of H-Ras in complex with Raf	(Fetics et al., 2015)	PDB ID: 4G0N

REAGENT or RESOURCE	SOURCE	IDENTIFIER
Crystal structure of Ras homolog domain p190RhoGAP bound to GNP	Structural Genomics Consortium	PDB ID: 3C5H
Oligonucleotides		
Primers for cloning and mutagenesis, see Table S1	This paper	N/A
Recombinant DNA		
pGEX-6p1	GE Healthcare	Cat#28954648
modified pET vector	This paper	N/A
pCDFDuet-1	Millipore Sigma	Cat#71340-3
p190RhoGAP-A (rat)	This paper	NCBI NP_001258061.1
Rac1 (human)	(Davis et al., 2013)	UniProt ID: P63000
Rnd3 (human)	This paper	UniProt ID: P61587
H-Ras (human)	This paper	UniProt ID: P01112
Software and Algorithms		
SBGrid	(Morin et al., 2013)	https://sbgrid.org/
XDS	(Kabsch, 2010)	http://xds.mpimf-heidelberg.mpg.de/
PHENIX	(Adams et al., 2010; Afonine et al., 2012)	https://www.phenix-online.org/
coot	(Emsley et al., 2010)	https://www2.mrc-lmb.cam.ac.uk/personal/pemsley/coot/
CCP4mg	(McNicholas et al., 2011)	http://www.ccp4.ac.uk/MG/